

Theory and Fundamental Limit of Quasiachromatic Metalens by Phase Delay Extension

Qikai Chen^{1,2}, Yubin Gao^{1,2}, Sijie Pian^{1,2} and Yaoguang Ma^{1,2,3,*}

¹State Key Laboratory of Extreme Photonics and Instrumentation, College of Optical Science and Engineering, International Research Center for Advanced Photonics, Zhejiang University, Hangzhou 310058, China

²ZJU-Hangzhou Global Scientific and Technological Innovation Center, Hangzhou, 311200, China

³Jiaxing Key Laboratory of Photonic Sensing and Intelligent Imaging, Intelligent Optics and Photonics Research Center, Jiaxing Research Institute, Zhejiang University, Jiaxing, 314000, China



(Received 18 May 2023; accepted 3 October 2023; published 7 November 2023)

The periodic extension of phase difference is commonly applied in device design to obtain phase compensation beyond the system's original phase modulation capabilities. Based on this extension approach, we propose the application of quasiphase delay matching to extend the range of dispersion compensation for meta-atoms with limited height. Our theory expands the limit of frequency bandwidth coverage and relaxes the constraints of aperture, NA, and bandwidth for metalenses. By applying the uncertainty principle, we explain the fundamental limit of this achromatic bandwidth and obtain the achromatic spectrum using perturbation analysis. To demonstrate the effectiveness of this extended limit, we simulate a quasiachromatic metalens with a diameter of 2 mm and a NA of 0.55 in the range of 400–1500 nm. Our findings provide a novel theory for correcting chromatic aberration in large-diameter ultrawide bandwidth devices.

DOI: [10.1103/PhysRevLett.131.193801](https://doi.org/10.1103/PhysRevLett.131.193801)

Achromatic metalenses (AMLs) have been extensively studied for compact optical systems [1–5]. Recent methods range from multiple wavelengths AMLs based on initial phase optimization [6,7] to broadband achromatic metalenses (BAMLs) based on compensating phase profiles with waveguidelike dispersion [5,8–11]. However, the chromatic aberration correction of metalenses is still constrained by a balance between aperture, NA, and bandwidth, making it challenging to meet the dispersion requirements of large NAs and apertures with low meta-atom height. Therefore, it is crucial to break the constraint and establish fundamental limit of AMLs.

Several approaches have been explored to extend the achromatic bandwidth of AMLs, such as using high aspect ratios [11] or multilayer structures [12–15]. However, these approaches requires meta-atoms with millimeter height for large apertures and high NAs, thus encounter fabrication and design challenges in achieving the required dispersion compensation. Other approaches utilized folded group delay profiles [16] to reduce the requirements for height of meta-atoms while maintaining gradient of profile. Such methods [17] optimize multiwavelength phase profile by introducing nonideal phase condition, which alters the shape of the focal wavefront and provides more design degrees of freedom. Although AMLs designed by deep learning and inverse design [18,19] demonstrate high-quality imaging performance with reconstruction algorithms [20], they have not addressed the theoretical analysis of achromatic spectrum and the fundamental bandwidth limitations. In this Letter, we present a novel approach to

extend the bandwidth limit of achromatic devices with ultralarge dispersion requirements. Our method utilizes phase delay extension to broaden the achromatic spectrum of AMLs while preserving the height of the meta-atoms. To validate our approach, we conduct simulations to compare its performance with that of published works.

Metalenses are typically based on a hyperbolic phase profile [1], where the phase response of meta-atoms ϕ_{atom} must be extended to match ϕ_{lens} in large aperture metalenses as

$$\begin{aligned}\phi_{\text{lens}}(r, \omega) &= \phi_{\text{atom}}(r, \omega) + m_{\phi}(r, \omega) \cdot 2\pi, \\ \phi_{\text{atom}}(r, \omega) &= \text{mod}(\phi_{\text{lens}}(r, \omega), 2\pi).\end{aligned}\quad (1)$$

Here, r represents the location on metalens, m_{ϕ} represents the numbers of phase extensions [see Fig. 1(a)]. To fully represent the step function in Eq. (1), we express the phase difference between phase profiles of different frequencies by phase delay (PD) with respect to central frequency ω_0 . In this case, the achromatic condition of PD can also be expressed as a hyperbolic function.

$$\begin{aligned}\text{PD}(r, \omega) &= \frac{\phi_{\text{lens}}(r, \omega) - \phi_{\text{lens}}(r, \omega_0)}{\omega - \omega_0} \\ &= -\frac{1}{c} \left(\sqrt{F^2 + r^2} - F \right) + \frac{\phi_r(\omega) - \phi_r(\omega_0)}{\omega - \omega_0}.\end{aligned}\quad (2)$$

Here, F is the focal length, $\phi_r(\omega)$ represents the reference phase of phase profile at ω [6]. According to Eq. (2), the PD

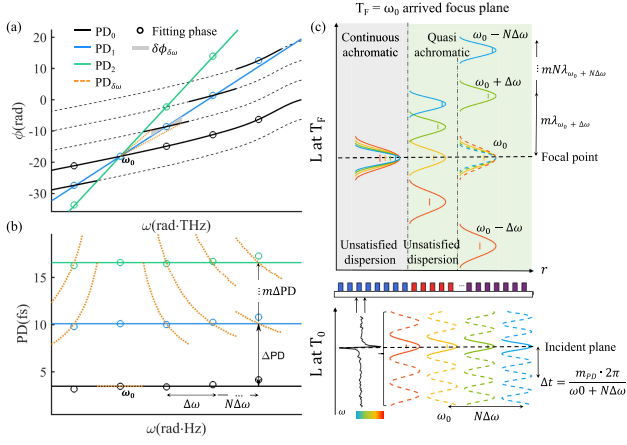


FIG. 1. (a) Phase extension with 2π interval between each pair of dashed lines. The stepped black lines represent the phase fitting at different frequencies. (b) PD extension. Blue and green lines represent $m = 1, 2$. The circles represent the phase extension points supported by the meta-atoms. The orange dashed curves represent PD curves at the entire frequency domain. (c) Schematic of achromatic focusing of PD extension. The upper part of QAML demonstrates the wave distribution at focusing time, and the bottom part at incident time. The solid color lines represent light incident at T_0 , while the dashed lines represent light incident at extended PDs.

requirements of BAML with large aperture and high NA often exceeds what can be supported by the meta-atoms, leading to strict aperture limitations for BAMLs with finite height of meta-atoms [7,21].

To provide a larger PD supported by meta-atoms, we leverage the relationship between PD and phase difference in Eq. (2), and propose that PD can also be extended with a period of $2\pi/\Delta\omega$ under specific frequency difference $\Delta\omega$. As shown in Fig. 1(b), the original PD line can be extended into the blue and green lines with an interval of $\Delta PD = 2\pi/\Delta\omega$. By mapping these lines onto phase plot, we obtain the corresponding phase response in Fig. 1(a) with different slopes of $PD_0 + 2m\pi/\Delta\omega, m = 1, 2$. Mathematically, we can always apply the PD extension at more frequencies $\omega = \omega_0 \pm N\Delta\omega (N = 1, 2, \dots)$ limited in the linear phase-frequency response region. Therefore, we can express the required phase difference modulation of the meta-atoms at these frequencies as

$$\Delta\phi_{N\Delta\omega}(r) = \text{mod}(PD(r), \Delta PD) \times N\Delta\omega + m_{PD}(r, \omega) \times 2\pi, \quad (3)$$

where the first item explains the minimum PD range (ΔPD) that meta-atoms needs to satisfy. With the PD extension, it is possible to fit the ultrawide PD profile using a limited PD range. We refer to this matching condition aimed at discrete frequencies $\omega_0 \pm N\Delta\omega$ as quasi-PD matching. The central phase $\phi_{\text{lens}}(r, \omega_0)$ can be achieved by the Berry phase [5,9,22] or by establishing a large database [7,11,23].

By selecting meta-atoms that simultaneously satisfy ϕ_0 and $\Delta\phi_{N\Delta\omega}$, we can perfectly meet achromatic conditions at $N_M = 2N + 1$ extended frequencies. (N_M is the total channel). We refer to metalenses that satisfies the half sampling channels of continuous spectrum as quasiachromatic metalenses (QAMLs). The equidistant frequencies obtained by QAMLs are similar as those of harmonic diffractive lenses [24,25], but maintain a more flexible design freedom when one chooses the central frequency ω_0 and frequency interval $\Delta\omega$, thus making QAMLs suitable for more application scenarios. QAMLs artificially introduce phase extensions m_{PD} at different positions and frequencies compared to BAMLs:

$$m_{PD}(r, \omega) \cdot 2\pi = \Delta m_\phi \cdot 2\pi = m(r)N(\omega) \cdot 2\pi$$

$$m(r) = \text{floor}(|PD(r)|/\Delta PD). \quad (4)$$

Here, $m(r)$ is a position-dependent natural number and $N(\omega)$ is a frequency-dependent natural number. Physically, the additional phase extensions actually affect the timing of waves entering the observing plane. As illustrated in Fig. 1(c), when $m(r) = 0$, all frequencies arrive at the focal point at the same time T_F . Whereas, in the region of large propagation dispersion (large NA or aperture), different frequencies are separated at T_F due to the inadequate PD of the meta-atoms. However, $m_{PD} \cdot 2\pi$ ensures that waves incident at $m_{PD} \cdot 2\pi/\omega$ before and after incident time T_0 focus simultaneously. Therefore, the incident signal before and after ΔPD can be utilized, reducing the actual time delay experienced by QAML:

$$\Delta T_{\text{QAML}}(r) = \frac{\Delta\phi_{\text{atom}}(r)}{N\Delta\omega} - \frac{\Delta\phi_{\text{atom}}(r=0)}{N\Delta\omega}$$

$$= \text{mod}(\Delta T_{\text{BAML}}(r), \Delta PD). \quad (5)$$

A significant advantage of this PD extension method is that receiving time for incident signals, ΔT_{QAML} , can be shorter compared to that of BAML, ΔT_{BAML} [21,26,27]. Where the maximum reception time duration is $\Delta T_{\text{QAML},\text{max}} = \Delta PD$. Therefore, the fundamental total bandwidth limit $\Delta\Omega$ of waveguide type QAML [27] is

$$\Delta PD \cdot \Delta\Omega \leq 2\pi \frac{h}{\lambda_0} (n_{\text{max}} - n_{\text{min}}). \quad (6)$$

Here, $\Delta\Omega$ is the standard deviation of spectral wave function. When the uncertainty principle is just satisfied [26], $\Delta\Omega\Delta t = 2$, the wave packet will be equivalent to Gaussian function. Since the frequencies in $\Delta\Omega_{\text{max}}$ cannot be distinguished, it can be defined as the fundamental bandwidth limit of QAML. The reception time ΔT_{QAML} is unaffected by the aperture and NA, thereby allowing for a more lenient height requirement of meta-atoms compared to BAML. Moreover, this feature enables an extended bandwidth limit for larger lens apertures. The reception time

ΔT_{QAML} is unaffected by the aperture and NA, thereby allowing for a more lenient height requirement of meta-atoms compared to BAML. Moreover, this feature enables an extended bandwidth limit for larger lens apertures.

We also evaluated the achromatic performance of this method under a frequency perturbation $\delta\omega$ around $\omega_0 \pm N\Delta\omega$, and a perturbation δPD around extended PD. These perturbations will introduce phase mismatches to Eq. (3) [see Fig. 1(a)], which are critical factors limiting the achromatic ability. The expression for phase mismatch is given by

$$\delta\phi(r) = 2m(r)\pi \frac{\delta\omega}{\Delta\omega} + \delta\text{PD}(r) \cdot N\Delta\omega, \quad (7)$$

where we neglected the coupling term of the two perturbation $\delta\text{PD} \cdot \delta\omega$. Considering only the frequency perturbation, we define the phase mismatch

$$\delta\phi_{\delta\omega}(r) = 2m(r)\pi \frac{\delta\omega}{\Delta\omega}. \quad (8)$$

Thus, we substitute $\delta\phi_{\delta\omega}$ into the Fresnel diffraction and obtain the electric field amplitude at focal point. Assuming that the transmittance of all meta-atoms is 1, we calculate the ratio of the amplitude under perturbation to that without mismatch as

$$\begin{aligned} & \frac{|E_F(\omega + N\Delta\omega + \delta\omega)|}{E_F(\omega + N\Delta\omega)} \\ &= \left| \frac{\sum_{m=0}^{M-1} e^{i2m\pi\delta\omega/\Delta\omega} + (f_{\max} - M) \cdot e^{i2M\pi\delta\omega/\Delta\omega}}{f_{\max}} \right| \\ &\equiv \text{Ratio}_1(\delta\omega) \end{aligned} \quad (9)$$

$$f_{\max} = \frac{\left(\sqrt{F^2 + \left(\frac{D}{2}\right)^2} - F\right)}{c\Delta\text{PD}},$$

where $M = m_{\max}$ represents the maximum PD extension number. When $\text{Ratio}_1 = 0.89$, Eq. (9) is equivalent to the Rayleigh criterion, and $\delta\omega_R$ obtained at this ratio represents the achromatic sub-bandwidth at $\omega_0 \pm N\Delta\omega$, where frequencies within $\delta\omega_R$ cannot be distinguished [28]. We assume that phase mismatch does not affect the focusing efficiency, but only the focal length. This assumption is particularly stringent because, when considering other aberrations, the nonideal shape of the Airy disk necessitates the consideration of lower focusing efficiency. This leads to a relaxed Rayleigh criterion with lower Ratio_1 , resulting in a wider calculated achromatic sub-bandwidth. As $\delta\omega$ increases, we can obtain the PD curve at the entire frequency domain [see Fig. 1(b)]. This enables us to identify the dispersion requirements that materials need

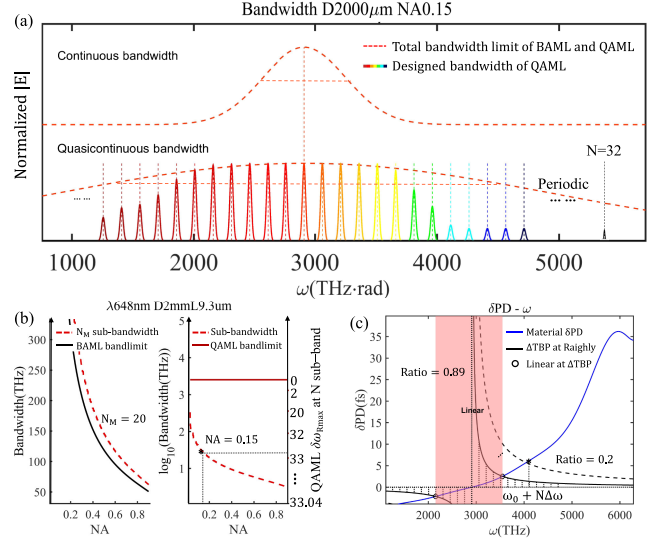


FIG. 2. (a) Achromatic spectrum of QAML and BAML bandwidth limit. The colored dashed line represents the ideal achromatic amplitude under flat spectrum input without nonlinear dispersion. (b) Comparison of bandwidth of QAML and BAML with their limits, where the QAML total sub-bandwidth exceeds the BAML bandwidth limit when $N_M = 20$. The fundamental bandwidth limit of sub-band $\delta\omega_R$ is also dependent to N . (c) Nonlinear dispersion analysis. The red region determined by the Raleigh criterion represents linear dispersion region.

to meet under the achromatic condition. Moreover, When $M = 0$, the phase mismatch in Eq. (9) can be eliminated, leading to the case of BAMLs. While at $M = 2$, the tails of subpeaks are merely connected, demonstrating a continuous sampling achromatic spectrum. The different extent of PD extension showing a wide applicability of QAML on spectral modulation under fundamental limit.

By calculating Ratio_1 at different frequencies, we plot the normalized achromatic spectrum of QAML with a flat spectrum incidence in Fig. 2(a) (aperture $D = 2$ mm and $\text{NA} = 0.15$). Furthermore, we compared the achromatic spectrum under maximum bandwidth of BAML and QAML with the same conditions. In Fig. 2(b), we compare the total sub-bandwidth with $N_M = 20$, sub-band of QAML, and the bandwidth limit of BAML. All the results consistently demonstrate the significant advantages of QAML under the wide spectral input and large aperture.

The achromatic spectrum is also affected by δPD arising from the nonlinear dispersion of material. Assuming that δPD_{\max} of the meta-atom is linearly proportional to its filling factor [29,30], the nonlinear dispersion phase mismatch can be expressed as

$$\begin{aligned} \delta\phi_{\delta\text{PD}}(r) &= \delta\text{PD}(r) \cdot N\Delta\omega \\ &= \delta\text{PD}_{\max} \cdot \text{mod}(\text{PD}(r), \Delta\text{PD}) / \Delta\text{PD} \cdot N\Delta\omega. \end{aligned} \quad (10)$$

Similarly, we obtain normalized amplitude Ratio_2 .

$$\begin{aligned} & \frac{|E_{F,\delta\text{PD}}(\omega + N\Delta\omega)|}{|E_F(\omega + N\Delta\omega)|} \\ &= \left| \frac{M(1 - e^{i\Delta\text{TBP}}) + e^{i\Delta\text{TBP}(-f_{\text{max}}+M+1)} - e^{i\Delta\text{TBP}}}{-i\Delta\text{TBP}f_{\text{max}}} \right| \\ &\equiv \text{Ratio}_2(\delta\text{PD}) \end{aligned} \quad (11)$$

$$\Delta\text{TBP} = \delta\text{PD}_{\text{max}} \cdot N\Delta\omega.$$

In Eq. (11), we define the nonlinear tolerable time-bandwidth product as ΔTBP , which indicates the extent to which QAML tolerates $\delta\text{PD}_{\text{max}}$ at $\omega_0 \pm N\Delta\omega$. Thus, based on the material's δPD and ΔTBP at the Rayleigh criterion [see Fig. 2(c)], this method proves highly effective in optimizing the linearity of the phase-frequency response of meta-atoms. Considering the nonlinear dispersion by Ratio_2 , we amended the normalized amplitude of spectrum in Fig. 2(a). This method of analyzing nonlinear dispersion is not only applicable to QAMLs, but also valuable for other AMLs.

The fundamental limit on the wave function altered by quasiachromatic condition is also evaluated. We use the Cauchy dispersion formula to relate δPD and refractive index at frequencies far from the resonant absorption. Besides, assuming the wave function can be fully defined as equidistant peaks with a consistent sub-bandwidth in the linear region, we obtain the fundamental bandwidth limit of sub-bandwidth as

$$(2N + 1)\delta\omega_{\text{R}}^2 + \frac{1}{3}N(N + 1)\Delta\omega^2 < \omega_0^2 \cdot \left(\frac{\delta\text{PD}_{\text{max}}}{\Delta\text{PD}} + 1 \right)^2, \quad (12)$$

where the influence of δPD is neglected on the left, resulting in a more stringent limit. Thus, we relate the fundamental limit $\Delta\Omega_{\text{max}}$ to each sub-bandwidth, and express the maximum achievable achromatic sub-bandwidth as $\delta\omega_{\text{Rmax}}$. Moreover, $\delta\omega_{\text{Rmax}}$ is equal to $\Delta\Omega_{\text{max}}$ when $N = 0$, and decreases as N increases [see Fig. 2(b)]. For our QAML, $\delta\omega_{\text{Rmax}}$ become closer to the sub-bandwidth $\delta\omega_{\text{R}}$ at $N \geq 32$. Since this limit is only attainable when the spectrum is equivalent to a Gaussian function, it begins to affect the achromatic spectrum by

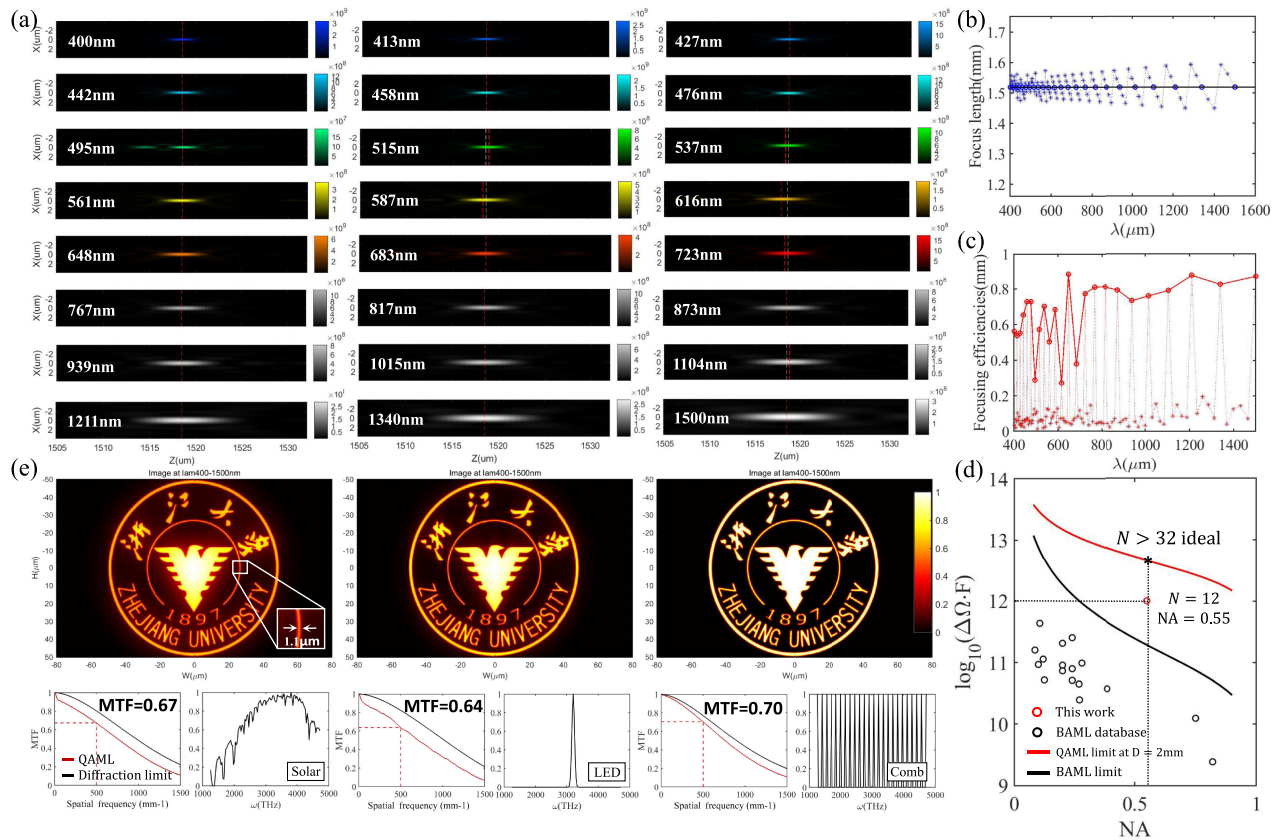


FIG. 3. (a) PSFs of QAML at extended frequencies. (b),(c) Focal lengths and focusing efficiencies of PSF at all frequencies. The star points represent deviation frequencies, and the focusing efficiency is obtained from the energy within 3 times the Airy disk radius. (d) Comparisons of published BAML database [12] and fundamental bandwidth limit of BAMLs and QAMLs. (e) Simulated normalized pseudoimaging results and MTFs under solar spectrum, LED, and optical frequency comb incident, respectively.

concentrating peaks on certain frequencies, thereby reducing the standard deviation of the wave function. However, for QAML with a flat spectrum incidence, the decreased normalized amplitude at other frequencies indicates that the energy spreads out from focal point, leading to a decrease in the focusing efficiency and poorer achromatic capability. Nonetheless, the effect of δPD already becomes significant when $N = 12$, therefore plays a decisive role in limiting achromatic spectrum.

To verify the theory of PD extension, we designed a QAML with a large aperture $D = 2000 \mu\text{m}$ and a high NA of 0.55. We selected 24 extension frequencies in 400–1500 nm to achieve near-continuous sampling. The period of rectangular meta-atoms was $P = 420 \text{ nm}$. TiO_2 was chosen as the material in finite-difference time domain and the minimum height of the waveguidelike meta-atoms [2,31] was determined as $L = 9.3 \mu\text{m}$ to satisfy required $\Delta PD = 42 \text{ fs}$. We calculate the far-field propagation at extension frequencies [see Fig. 3(a)], all incident frequencies were focused at the designed focal plane.

Furthermore, we simulated focal lengths for 116 frequencies within the selected band [see Fig. 3(b)]. Notably, the deviation of focal lengths at $\omega_0 \pm N\Delta\omega$ are less than 0.1%, demonstrating remarkable achromatic performance. In addition, we calculated their focusing efficiencies [see Fig. 3(c)] and found that the average focusing efficiency remained above 65%. Moreover, the focusing efficiencies at deviation frequencies were extremely low, indicating a negligible impact on imaging results. We also compared the bandwidth with published BAMLs and their limitations. As predicted earlier, the bandwidth of QAML far exceeded the limit of BAML under $N = 12$. Using materials with better linearity of phase-frequency response, we can approach the fundamental limit at $N = 32$.

We further obtained their corresponding point spread function (PSFs) and modulation transfer function (MTFs). Subsequently, by convolving the PSF with the object image at different frequencies, we calculated the pseudoimaging results in the full spectrum. Solar spectrum, LED spectrum centered at 590 nm with a FWHM of 75 nm, and comb spectrum that fully satisfied the extended frequencies were adopted as light sources [see Fig. 3(e)]. Notably, comb incidence yielded the most optimal imaging results with a near diffraction-limit MTF. As the spectrum widens, nonoptimized frequencies result in stray light in the imaging plane, but remains within an acceptable range with high MTFs, demonstrating a promising imaging application. When the size of the imaging plane is set to $120 \times 160 \mu\text{m}$, the imaging resolution of QAML under the incidents with different spectrums is close to the theoretical Airy disk diameter of $1.1 \mu\text{m}$ for $\lambda = 0.49 \mu\text{m}$, which is quite ideal.

In this Letter, we propose a promising method for achromatic optics and derive the fundamental limitations of QAMLs. Our phase delay extension method overcomes

the limited dispersion ability of meta-atoms with limited height, and relaxes the constraints between bandwidth, NA, and aperture. This approach provides a theoretical foundation for achieving ultrawide spectrum and large-aperture achromatic components in the future, which will advance the development of achromatic compact optical systems, including grating and optical vortex devices. While QAML effectively circumvent the unattainable height requirements of BAML under large apertures and high NA, challenges persist when dealing with small frequency interval $\Delta\omega$. QAMLs still need to address fabrication considerations such as high aspect ratios and stringent precision requirements. Upon resolution of these challenges, QAMLs, with their ultrawide bandwidth capabilities achieved through PD extension, hold great promise for advanced imaging applications in aerospace remote sensing, geological exploration, medical detection, and other well-established fields of diffractive optics, both in military and civilian domains. Consequently, QAMLs represent an exciting development with significant potential for revolutionizing various fields of science and technology.

The authors acknowledge Professor Xu Liu and Professor Cuifang Kuang for encouragement, support, and vision. Funding: This work is supported by the National Natural Science Foundation of China (NSFC) (62222511), STI 2030–Major Projects 2021ZD0200401, Natural Science Foundation of Zhejiang Province China (LR22F050006).

Y. M. and Q. C. conceived the idea. Q. C. performed the modeling, simulation, data analysis. Y. G. and S. P. assisted the simulation and data analysis. All authors contributed to the discussion of the manuscript. Y. M. supervised the research project.

*Corresponding author: mayaoguang@zju.edu.cn

- [1] M. Khorasaninejad, W. T. Chen, R. C. Devlin, J. Oh, A. Y. Zhu, and F. Capasso, *Science* **352**, 1190 (2016).
- [2] M. Khorasaninejad, A. Y. Zhu, C. Roques-Carmes, W. T. Chen, J. Oh, I. Mishra, R. C. Devlin, and F. Capasso, *Nano Lett.* **16**, 7229 (2016).
- [3] R. J. Lin, V.-C. Su, S. Wang, M. K. Chen, T. L. Chung, Y. H. Chen, H. Y. Kuo, J.-W. Chen, J. Chen, Y.-T. Huang, J.-H. Wang, C. H. Chu, P. C. Wu, T. Li, Z. Wang, S. Zhu, and D. P. Tsai, *Nat. Nanotechnol.* **14**, 227 (2019).
- [4] G. Yoon, K. Kim, D. Huh, H. Lee, and J. Rho, *Nat. Commun.* **11**, 2268 (2020).
- [5] S. Wang, P. C. Wu, V.-C. Su, Y.-C. Lai, C. Hung Chu, J.-W. Chen, S.-H. Lu, J. Chen, B. Xu, C.-H. Kuan, T. Li, S. Zhu, and D. P. Tsai, *Nat. Commun.* **8**, 187 (2017).
- [6] M. Khorasaninejad, Z. Shi, A. Y. Zhu, W. T. Chen, V. Sanjeev, A. Zaidi, and F. Capasso, *Nano Lett.* **17**, 1819 (2017).
- [7] S. Shrestha, A. C. Overvig, M. Lu, A. Stein, and N. Yu, *Light. Light.* **7**, 85 (2018).

- [8] W. T. Chen, A. Y. Zhu, V. Sanjeev, M. Khorasaninejad, Z. Shi, E. Lee, and F. Capasso, *Nat. Nanotechnol.* **13**, 220 (2018).
- [9] S. Wang, P. C. Wu, V.-C. Su, Y.-C. Lai, M.-K. Chen, H. Y. Kuo, B. H. Chen, Y. H. Chen, T.-T. Huang, J.-H. Wang, R.-M. Lin, C.-H. Kuan, T. Li, Z. Wang, S. Zhu, and D. P. Tsai, *Nat. Nanotechnol.* **13**, 227 (2018).
- [10] Z.-B. Fan, H.-Y. Qiu, H.-L. Zhang, X.-N. Pang, L.-D. Zhou, L. Liu, H. Ren, Q.-H. Wang, and J.-W. Dong, *Light. Light.* **8**, 67 (2019).
- [11] Y. Wang, Q. Chen, W. Yang, Z. Ji, L. Jin, X. Ma, Q. Song, A. Boltasseva, J. Han, V. M. Shalaev, and S. Xiao, *Nat. Commun.* **12**, 5560 (2021).
- [12] Q. Chen, Y. Liu, Y. Lei, S. Pian, Z. Wang, and a. Y. Ma, *Prog. Electromagn. Res.* **173**, 9 (2022).
- [13] F. Balli, M. Sultan, S. K. Lami, and J. T. Hastings, *Nat. Commun.* **11**, 3892 (2020).
- [14] M. Li, S. Li, L. K. Chin, L. K. Chin, Y. Yu, Y. Yu, D. P. Tsai, R. Chen, and R. Chen, *Opt. Express* **28**, 26041 (2020).
- [15] O. Avayu, E. Almeida, Y. Prior, and T. Ellenbogen, *Nat. Commun.* **8**, 14992 (2017).
- [16] Z. Li, P. Lin, Y.-W. Huang, J.-S. Park, W. T. Chen, Z. Shi, C.-W. Qiu, J.-X. Cheng, and F. Capasso, *Sci. Adv.* **7**, eabe4458 (2021).
- [17] X. Xiao, Y. Zhao, X. Ye, C. Chen, X. Lu, Y. Rong, J. Deng, G. Li, S. Zhu, and T. Li, *Light. Light.* **11**, 323 (2022).
- [18] Y. Gao, Q. Chen, S. Pian, and Y. Ma, *Photonics Nanostruct. Fundam. Appl.* **52**, 101074 (2022).
- [19] Z. Li, R. Pestourie, J.-S. Park, Y.-W. Huang, S. G. Johnson, and F. Capasso, *Nat. Commun.* **13**, 2409 (2022).
- [20] E. Tseng, S. Colburn, J. Whitehead, L. Huang, S.-H. Baek, A. Majumdar, and F. Heide, *Nat. Commun.* **12**, 6493 (2021).
- [21] F. Presutti and F. Monticone, *Optica* **7**, 624 (2020).
- [22] M. Khorasaninejad, W. T. Chen, A. Y. Zhu, J. Oh, R. C. Devlin, C. Roques-Carnes, I. Mishra, and F. Capasso, *IEEE J. Sel. Top. Quantum Electron.* **23**, 43 (2017).
- [23] A. Ndao, L. Hsu, J. Ha, J.-H. Park, C. Chang-Hasnain, and B. Kanté, *Nat. Commun.* **11**, 3205 (2020).
- [24] S. Sinzinger and M. Testorf, *Appl. Opt.* **34**, 5970 (1995).
- [25] D. W. Sweeney and G. E. Sommargren, *Appl. Opt.* **34**, 2469 (1995).
- [26] David A. B. Miller, *Phys. Rev. Lett.* **99**, 203903 (2007).
- [27] R. S. Tucker, P.-C. Ku, and C. J. Chang-Hasnain, *J. Light-wave Technol.* **23**, 4046 (2005).
- [28] See Supplemental Material at <http://link.aps.org/supplemental/10.1103/PhysRevLett.131.193801> for detailed derivation of equations, simulation results and comparison with HDLs.
- [29] J. Shin, J.-T. Shen, and S. Fan, *Phys. Rev. Lett.* **102**, 093903 (2009).
- [30] E. Bayati, A. Zhan, S. Colburn, and A. Majumdar, *Appl. Opt.* **58**, 1460 (2019).
- [31] M. Khorasaninejad and F. Capasso, *Science* **358**, eaam8100 (2017).